2017

Design Analysis of Subwavelength Gratings as VCSEL Mirrors

Austin M. Slosberg
Lehigh University

Design Analysis of Subwavelength Gratings as VCSEL Mirrors

by

Austin M. Slosberg

A Thesis

Presented to the Graduate and Research Committee

Of Lehigh University

In Candidacy for the Degree of

Master of Science

In

Electrical Engineering

Lehigh University

December 2017

This thesis is accepted and approved in partial fulfillment of the requirements for a Master's of Science.

Date: December 6th 2017

Prof. Nelson Tansu, MS Thesis Advisor

Daniel E. '39 and Patricia M. Smith Endowed Chair Professor

Director, Center for Photonics and Nanoelectronics

Prof. Chengshan Xiao

Chair of Electrical and Computer Engineering Department

Acknowledgement

I would like to thank my advisor Professor Nelson Tansu for not only guiding me through my research here, but also giving me the opportunity to work in a fantastic group of people. Before coming to Lehigh, I felt I didn't have a direction in life and my teachers and friends here have been my compass. It is with great pride in myself and those I've gotten to know that I submit this thesis as only a tiny fraction of what I've been taught by all my colleagues here. I feel it would be redundant to name everyone important to me here, but everyone who works in or with Professor Tansu's group has a spot on that list.

I am thankful for my family for financially and emotionally supporting me through all my undergraduate and graduate studies as well as supplying me with free and homecooked food when I come home. I want to acknowledge my cousin, future Juris Doctor and professional gamer Cody Schwab, for the never ending facebook messages and memes. Last but definitely not least I want to show my appreciation to my best friends Justin Zwick and Edmund Dalton whom I've known since kindergarten and 9th grade respectively. While most students when far from home call their parents every day, I called them. Through my best and worst times here there was never a time I couldn't count on them to make me smile and I am forever thankful.

Table of Contents

List of Figures and Tables

Abstract

In this thesis, we examine the importance of an efficient mirror in laser structures regarding threshold current density, as well as proposed an alternative reflector in the form of Subwavelength Gratings (SWGs) to standard DBRs for III-Nitride VCSELs. The numerical method Rigorous Coupled Wave Analysis (RCWA) for grating reflectivity is shown and was used in all reflectivity simulations.

SWG reflectors for blue light of λ = 450 nm capable of ultra-high reflectivity were designed in this work, which is achievable by InGaN quantum well in III-Nitride VCSEL structures. This SWG is a GaN based grating on an air interface with a period (Λ), of 400 nm, a duty cycle of 50%, and a height (H) of 130 nm which shows reflectivity >99% in the range of λ ~400 nm to ~460 nm. This grating is polarization selective and favors reflecting TE light, where the electric field is parallel to the grating bars. The effect of variations in grating period, height, and duty cycle were explored and it was found the period has a significant impact on the position of the reflective band. A threshold analysis was performed on a VCSEL implementing the designed SWG and threshold current densities of ~ 4.6 kA/cm^2 were achieved for a light emission of 450 nm. This grating mirror is designed with the intent of replacing the inefficient p-type DBRs in standard III-Nitride VCSEL structures, and was shown to be an exceptional upgrade. Lastly a fabrication for our membrane structure SWG was proposed.

1. Vertical Cavity Surface Emitting Lasers (VCSELs)

1.1. The First Steps of VCSELs

VCSELs were first conceived by Kenichi Iga and his group in 1977 with an eventual device realization in 1979 [1], [2]. As the name suggests light emits from the VCSEL's surface as opposed to edge emitting lasers which emit light from the side of the laser structure. While the initial devices had incredibly short lifetimes, a new field was opened, leading to the first GaAs based continuous wave operation VCSEL in 1988 [1]. Figure 1-1 demonstrates the low threshold currents of VCSEL structures, which can be attributed to a small active volume in QW VCSELs resulting in much lower threshold currents than in plane lasers, as low as multiple milliamperes [3], [4]. VCSELs hold multiple advantages over edge emitters such as single mode output, practical coupling to optical fibers, 2D array integration, etc [1].

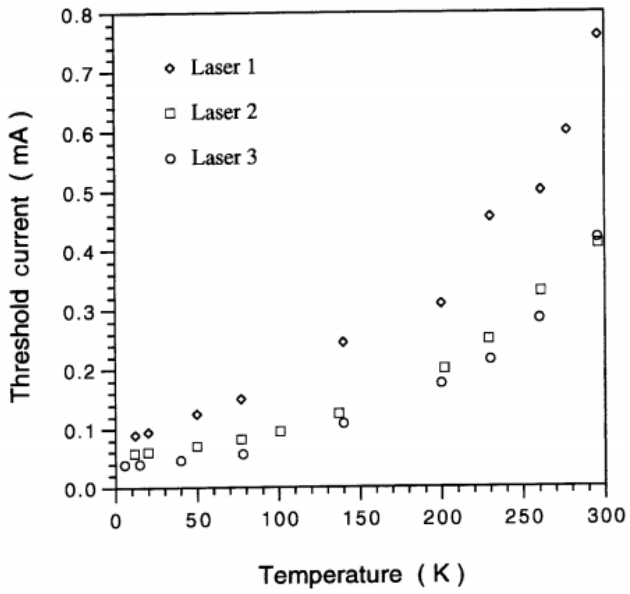

Figure 1-1: Threshold currents as a function of ambient temperature for single QW InGaAs lasers with various mirror coatings [3].

1.2. VCSEL Structures

In its most basic form a VCSEL is comprised of an active region (commonly a quantum well or multiple quantum wells) encompassed by p-type and n-type barriers forming a λ cavity which is all surrounded by the top and bottom p-type and n-type mirrors. Many laser designs for both VCSELs and edge emitters utilize Distributed Bragg Reflectors (DBRs) as the mirrors surrounding the cavity [1], [5]. An illustration of a basic VCSEL structure is shown in figure 1-2. The purpose of the λ cavity, which is an integer multiple of λ in length, is to allow a standing wave for the desired lasing wavelength. This small cavity size is not achievable for in plane lasers and leads to very selective single mode output for VCSELs.

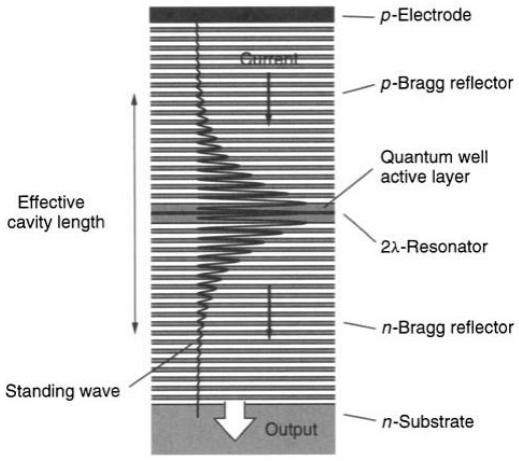

Figure 1-2: An illustration of a VCSEL structure highlighting the substrate, p-type and n-type DBRs, as well as the active region and λ cavity.

A single DBR is comprised of two transparent dielectric slabs, usually with a large index contrast, that are both a quarter of the wavelength of light in the material which needs to be reflected. While a single DBR does not exhibit very high reflectivity, laser mirrors utilize many

(~30-50) DBRs allowing for ultra-high reflectivity with a large bandwidth at the desired wavelength. The reflectivity of a single DBR can be expressed by $R = \left|\frac{n_H + n_L}{n_{H-}\, n_L}\right|^2$. However, once there are multiple stacks of DBRs placed next to the p-type or n-type side of the λ cavity the reflectivity is expressed as shown in equation 1-1 [6].

$$R = \left|\frac{n_S f^{2N} - 1}{n_S f^{2N} + 1}\right|^2 \tag{1.2-1}$$

Where n_S is the index of refraction of the material in the λ cavity, f is $\frac{n_H}{n_L}$, and N is the number of DBR stacks in the system. With a suitable index contrast in f, the mirror reflectivity will exponentially rise with an increase in DBR pairs. The reflective bandwidth also increases with N, by equation 1-2 [6].

$$\Delta\lambda = \frac{4\lambda}{\pi} \sin^{-1} \frac{1 - f}{1 + f} \tag{1.2-2}$$

Where λ is the central wavelength and $\Delta\lambda$ is the total bandwidth of the central plateau as R approaches unity. Highly reflective mirrors are instrumental for fabrication of practical lasers. This stems from the reliance of a laser's threshold current density on the reflectivity of the top and bottom mirrors. Larger mirror reflectivity in the top and bottom mirrors will significantly reduce the mirror losses. Once the gain of the laser has surpassed the losses then the laser is said to have reached threshold. Threshold is the point when the system will begin to lase, producing a coherent and visible output from the laser facets. To find the threshold current density the first step is to find the threshold gain.

$$\Gamma g_{th} = \alpha_i + \alpha_m \tag{1.2-3}$$

Where α_i and α_m are the laser's intrinsic loss and mirror losses respectively and Γ is the confinement factor. Intrinsic losses are derived from material imperfections such as scattering, absorption, free carrier loss, etc [7]. The confinement factor is the proportion of light emitted from the active region that is confined in the cavity. Most light emitted from the active region is not confined in the laser cavity and instead leaves the system incoherently in all directions where there are no mirrors. Lastly the mirror losses result from the loss of light when travelling through the mirror and cavity of the system. The mirror losses can be expressed by

$$\alpha_m = \frac{1}{L}\ln\frac{1}{R_1 R_2} \tag{1.2-4}$$

Where L is the total length light in the system travels which includes the penetration depth into the mirrors as well as the λ cavity of the laser. R_1 and R_2 are the reflectivity of the top and bottom mirror which are both limited to a maximum reflectivity of 1. All losses are conventionally expressed in units of cm^{-1}. The threshold gain is related to the threshold carrier densities through

$$n_{th} = n_{tr} e^{\frac{g_{th}}{g_{0n}}} \tag{1.2-5}$$

Where n_{tr} is the transparent carrier density of the active region which is dependent on the material and material quality, g_{0n} is the differential gain and n_{th} is the threshold current density. Lastly there is a relation between the threshold carrier density and the threshold current density.

$$J_{th} = qt(An_{th} + Bn_{th}^2 + Cn_{th}^3) \tag{1.2-6}$$

A, B, and C are the various losses in semiconductor devices defined as the Shockley-Hall-Read (SHR) losses, spontaneous emission losses, and the auger losses respectively. Lastly 't' is the

thickness of the quantum well and q is the charge of an electron. VCSELs exhibit much larger threshold current densities due to the small area of their active regions, however they also exhibit lower threshold currents. The SHR losses occur due to material impurities causing trap energy levels between the band gap. The carriers and holes recombine in these traps and emit a phonon in the material. SHR recombination is most prevalent at low carrier densities, but becomes overshadowed by other losses at higher carrier densities. Spontaneous emission losses come from carriers in the conduction band recombining with holes by probability and not stimulated emission, which leads to incoherently produced photons of the same energy as the band gap. Spontaneous emission is the method by which LEDs emit light, but it hinders laser functionality and is most prevalent at medium carrier densities. Lastly Auger recombination occurs due to a recombination between a carrier and hole causing a transition of another carrier to a higher energy band and no light is emitted. This form of loss is seen at larger carrier densities and hinders high power efficiency.

1.3. Advantages of VCSELs

VCSELs are much smaller in size compared to edge emitting lasers. The active region area of a VCSEL is on the scale of ~5 μm^2 and can only be viewed via Scanning Electron Microscopy (SEM). The surface emitting property of VCSELs is what enables this immensely small size. In edge emitters, the laser cavity extends from the sides of the quantum well resulting in an extremely long cavity relative to VCSELs. The emission wavelengths of the laser are almost completely reliant on the cavity size.

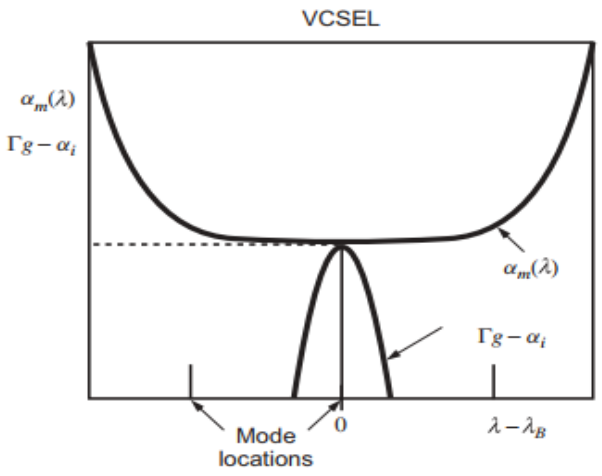

Figure 1-3a: Mode spacing, selection and mirror losses in VCSEL structures [30]. VCSELs exhibit single mode operation due to large mode spacing and narrow gain curves.

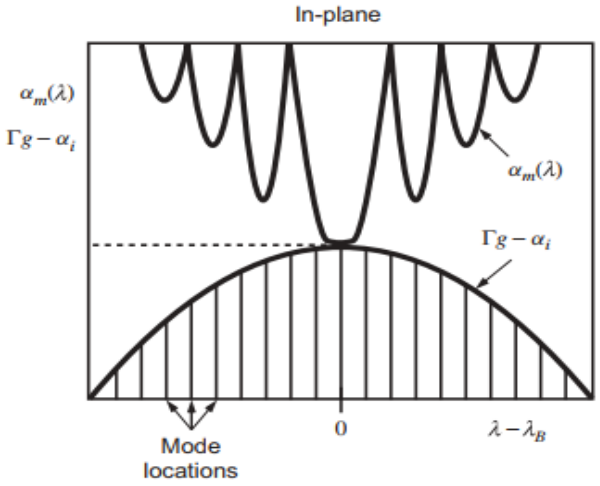

Figure 1-3b: Mode spacing, selection and mirror losses in in-plane structures [30]. Many modes are selected in these structures.

Figures 1-3a and 1-3b displace the mode spacing, gain curve, and mirror losses for VCSELs and in-plane lasers respectively. VCSELs exhibit single mode operation due to their small laser cavity while in-plane lasers will emit multiple modes of light during operation. The relationship between the mode spacing and the length of the cavity is given by equation 1-6.

$$d\lambda = \frac{\lambda^2}{2(\bar{n}_{ga}L_a + \bar{n}_{gp}L_p + \bar{n}_{gp}L_{eff})} \tag{1.3-1}$$

Where dλ is the mode spacing, $\bar{n}_{ga}$ is the group modal index of the active region, $\bar{n}_{gp}$ is the group modal index of the passive region, L_a and L_p are the lengths of the active and passive regions, and L_{eff} is the effective length of the mirror. The passive regions of VCSELs are much thinner than passive regions in in-plane lasers, leading to a much larger mode spacing. A larger mode spacing means less modes are present in the gain spectra, which makes single mode output possible.

The surface emitting quality of VCSELs allows practical integration into 2D arrays of hundreds or thousands of structures. These arrays preserve the power conversion efficiency of

the system while simultaneously increasing the output power. Thus, these arrays allow for efficient high power coherent laser beams. These beams can be coupled to optical fibers for efficient transmission of information or use in sensors.

1.4. Practical VCSELs

The practicality of a VCSEL is heavily dependent on the material quality and properties within its structure. Some materials are inherently better suited for the VCSEL designs discussed this chapter than others. Arsenide based materials have shown great promise in VCSEL practicality, while Nitride based materials have struggled. This is due to many reasons that will be discussed in depth later, however our focus is on the poor III-Nitride based DBR mirrors in VCSEL structures. We have shown that DBR mirrors have a significant impact on VCSEL practicality and thus III-Nitride VCSELs will require some alternative reflector which we propose to be in the form of a grating.

2. Rigorous Coupled Wave Analysis

2.1. RCWA Application and Implementation

The Rigorous Coupled Wave Analysis (RCWA) method is a computational method that analyzes modes of light in periodic structures using boundary equations at dielectric interfaces. This method is ideal for simulating reflectivity and transmission of light through grating structures because of their periodic property. In this section, the formulation of the RCWA method will be presented. Figure 2-1 shows an example of a grating structure that will be analyzed in this method. The focus of the formulation presented will be on incident TE light.

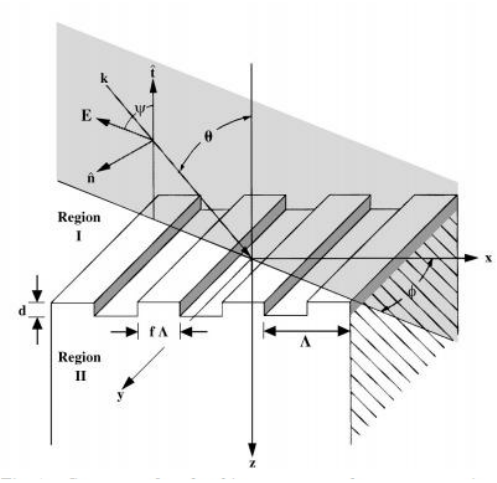

Figure 2-1: An illustration of a grating highlighting the grating height (d), period (Λ), duty cycle (f), angles of incidence (θ) and (ϕ), polarization angle (ψ), and the regions in and outside of the grating [8].

For this formulation, it is assumed that ϕ is 0 so there will be no conical diffraction in the system. In the grating region, the periodic relative permittivity can be expanded in a Fourier series in the form of equation 1.

$$\varepsilon(x) = \sum_{h} \varepsilon_h e^{i\frac{2\pi h}{\Lambda}} \tag{2.1-1}$$

In this equation, ε_h is the h^{th} Fourier component of the relative permittivity in the grating. The permittivity in the grating ridge region is harmonic and dependent on the duty cycle of the system. In the regions where there is a ridge and the regions in between the ridges there will be a different permittivity. These can be averaged and expressed by and can be expressed by equations 2.

$$\varepsilon_0 = n_{rd}^2 f + n_{gr}^2(1-f) \tag{2.1-2}$$

Where n_{rd} is the index of refraction of the ridges and n_{gr} is the index of refraction of the grooves. Also ε_h can be expressed by equation 3.

$$\varepsilon_h = (n_{rd}^2 - n_{gr}^2)\frac{\sin(\pi h f)}{\pi h} \tag{2.1-3}$$

The incoming electric field can be expressed by

$$E_{inc} = \exp\big(-jk_0 n_I(sin(\theta)x + cos(\theta)\, z)\big) = \exp(-jk_0 n_I z) \tag{2.1-4}$$

Where $k_0 = 2\pi/\lambda_0$ and n_I is the index of refraction in region one. λ_0 is the wavelength of light in free space. In the research presented in future chapters the focus is on normal incident light so an angle $\theta = 0^o$ is assumed. From here the electric fields in regions I and II are found by

$$E_I = E_{inc} + \sum_i R_i \exp(-j\big(k_{xi}x - k_{I,zi}z\big)) \tag{2.1-5}$$

$$E_{II} = \sum_i T_i \exp(-j\left(k_{xi}x - k_{II,zi}(z-d)\right)) \tag{2.1-6}$$

R_i and T_i are the normalized reflected and transmitted amplitudes of the i^{th} diffracted wave in regions I and II respectively. Where k_{xi} can be expressed by

$$k_{xi} = k_0(n_I \sin(\theta) - i\frac{\lambda_0}{\Lambda}) \tag{2.1-7}$$

$$k_{Li} = \begin{cases} k_0(n_L^2 - \left(\frac{k_{xi}}{k_0}\right)^2)^{\frac{1}{2}} & k_0 n_L > k_{xi} \\ -jk_0\left(\frac{k_{xi}}{k_0} - n_L^2\right)^{\frac{1}{2}} & k_0 n_L < k_{xi} \\ & L = I, II \end{cases} \tag{2.1-8}$$

In equation 7, L denotes the region of the grating interface. In the grating region, the electric field and magnetic fields can be expressed as

$$E_{gy} = \sum_i S_{yi}(z)\exp(-jk_{xi}x) \tag{2.1-9}$$

$$H_{gx} = -j\left(\frac{\epsilon_0}{\mu_0}\right)^{\frac{1}{2}} \sum_i U_{xi}(z)\exp(-jk_{xi}x) \tag{2.1-10}$$

Where μ_0 and ϵ_0 are the free space permeability and permittivity respectively. U_{xi} and S_{yi} are the normalized amplitudes of the i^{th} space harmonic fields. They are chosen such that E_{gy} and H_{gx} satisfy the equations

$$\frac{\partial E_{gy}}{\partial z} = j\omega\mu_0 H_{gx} \tag{2.1-11}$$

$$\frac{\partial H_{gx}}{\partial z} = j\omega\epsilon_0\varepsilon(x)E_{gy} + \frac{\partial H_{gz}}{\partial z} \tag{2.1-12}$$

Plugging in equations 8 and 9 into 10 and 11 and taking $\frac{\partial H_{gz}}{\partial z} = 0$ will give expressions for S_{yi} and U_{xi} as

$$\frac{\partial S_{yi}}{\partial z} = k_0 U_{xi} \tag{2.1-13}$$

$$\frac{\partial U_{xi}}{\partial z} = \left(\frac{k_{xi}^2}{k_0}\right) S_{yi} - k_0 \sum_p \varepsilon_{(i-p)} S_{yp} \tag{2.1-14}$$

It becomes convenient to solve these equations if they are instead expressed in matrix form. Assuming the matrix $A = K_x^2 - E$, where K_x is a diagonal matrix where every i^{th} element is comprised of k_{xi}/k_0 and E is the matrix where every i,p element is $\varepsilon_{(i-p)}$. Lastly the matrix equations are simplified further with a change of variables $z' = k_0 z$. From there the matrix equation can be expressed as

$$\begin{bmatrix} \frac{\partial S_y}{\partial z'} \\ \frac{\partial U_x}{\partial z'} \end{bmatrix} = \begin{bmatrix} 0 & I \\ A & 0 \end{bmatrix} \begin{bmatrix} S_y \\ U_x \end{bmatrix} \tag{2.1-15}$$

A substitution can be made using the relationship $\frac{\partial S_y}{\partial z'} = U_x$ and plugging back into $\frac{\partial U_x}{\partial z'} = S_y$ to obtain the relation

$$\left[\frac{\partial^2 S_y}{\partial z'^2}\right] = [A][S_y] \tag{2.1-16}$$

S_{yi} and U_{xi} can be solved by equations 14 and 15 and expressed by

$$S_{yi}(z) = \sum_{m=1}^{n} w_{i,m}(c_m^+ \exp(-k_0 q_m z) + c_m^- \exp(-k_0 q_m (d - z))) \tag{2.1-17}$$

$$U_{xi}(z) = \sum_{m=1}^{n} v_{i,m}(-c_m^+ \exp(-k_0 q_m z) + c_m^- \exp(-k_0 q_m (d - z))) \tag{2.1-18}$$

Where $w_{i,m}$ is the i,m positions in a matrix made of eigenvectors of A which will be denoted as W. The value q_m is the m^{th} position in a diagonal matrix comprised of the square root of the eigenvalues of A in a matrix that will be denoted as Q. From there $v_{i,m}$ can be defined as the i,m position of the matrix V = WQ. Lastly the constants c_m^+ and c_m^- are unknown constants that are determined from boundary conditions. We can solve for the fields R_i and T_i by these boundaries starting at the boundary z = 0.

$$\delta_{i0} + R_i = \sum_{m=1}^{n} w_{i,m}(c_m^+ + c_m^- \exp(-k_0 q_m d)) \tag{2.1-19}$$

$$j(n_I \cos\theta\, \delta_{i0} - R_i(\frac{k_{I,zi}}{k_0}) = \sum_{m=1}^{n} v_{i,m}(c_m^+ - c_m^- \exp(-k_0 q_m d)) \tag{2.1-20}$$

And taking the boundary at z = d gives

$$T_i = \sum_{m=1}^{n} w_{i,m}(c_m^+ \exp(-k_0 q_m d) + c_m^-) \tag{2.1-21}$$

$$j(\frac{k_{II,zi}}{k_0})T_i = \sum_{m=1}^{n} v_{i,m}(c_m^+ \exp(-k_0 q_m d) - c_m^-) \tag{2.1-22}$$

Equations 17-20 setup 2 matrix equations for T_i and R_i in terms of the unknown values c_m^+ and c_m^-.

$$\begin{bmatrix} \delta_{io} \\ jn_I\delta_{io} \end{bmatrix} + \begin{bmatrix} I \\ -jY_I \end{bmatrix}[R] = \begin{bmatrix} W & WX \\ V & -VX \end{bmatrix}\begin{bmatrix} c^+ \\ c^- \end{bmatrix} \tag{2.1-23}$$

$$\begin{bmatrix} I \\ jY_{II} \end{bmatrix}[T] = \begin{bmatrix} WX & W \\ VX & -V \end{bmatrix}\begin{bmatrix} c^+ \\ c^- \end{bmatrix} \tag{2.1-24}$$

The cos(θ) term vanishes when we assume θ = 90^0 Where δ_{i0} = 1 if i = 0 and δ_{i0} = 0 otherwise. X is defined as a diagonal matrix of elements $\exp(-k_0 q_m d)$. Lastly Y_L is the diagonal matrix of $\frac{k_{L,zi}}{k_0}$ where L = I,II. Lastly the diffraction efficiencies are defined as

$$DE_{ri} = R_i R_i^* Re\left(\frac{k_{I,zi}}{k_0 n_I}\right) \tag{2.1-25}$$

$$DE_{ti} = T_i T_i^* Re\left(\frac{k_{II,zi}}{k_0 n_I}\right) \tag{2.1-26}$$

For the studied gratings in this work the reflectivity is at i = (n+1)/2 and all other diffracted orders are 0. For lossless gratings energy conservation applies and $DE_{ti} + DE_{ri} = 1$. This method is proposed by M. G. Moharam [8], other works have built upon this method for further numerical stability and other systems [9], [10].

2.2. RCWA Application to VCSELs

We have shown the basis of the RCWA method regarding the interaction between light and a grating. These equations are the beginning of the method used to determine the reflectivity of our grating reflectors, and have been used for all reflectivity simulations in this work. Our RCWA code considers the properties of the grating as well as a dielectric slab on above and below the grating. We take the slab on the exit plane of the grating to be air as our grating requires it as we will discuss later, and the slab on the input plane to be air or even other materials. This allows us to simulate the effectiveness of our grating as a mirror and eventually as an implemented piece in the VCSEL structure.

3. Subwavelength Gratings

3.1. What are SWGs?

SWGs have shown remarkable reflectivity (>99%) in the infrared [11]–[21] and the blue light spectrum [22]. Broadband reflectivity in the infrared region has been achieved with a bandwidth of $\Delta\lambda/\lambda$~ 30% for R>99%. GaAs VCSEL structures have successfully implemented SWG mirrors for the infrared spectrum, but there have been no known attempts for GaN VCSELs implementing SWGs for blue light reflection. An SWG with the correct period (Λ), duty cycle, height, and the high and low index of refractions as shown in figure 1, will exhibit immense and broad reflectivity for a desired spectral regime. To achieve ultra-high reflectivity in any spectral regime, the physical dimensions of the grating need to be near but smaller than the wavelength of light reflected. SWGs also possess a benefit towards the series resistance of the VCSEL structure. At each DBR interface an electric field is produced which builds a resistance that won't be present when utilizing an SWG. There have been multiple explanations for the reflective property of SWGs such as resonance reflection driven by reradiation and excitation of lateral Bloch modes via the +- 1 evanescent diffraction orders [20] ,as well as waveguide properties due to the dimensions of the grating which cause the activated modes of light to deconstructively interfere on the exit plane resulting in no power transmitted and total reflection [14].

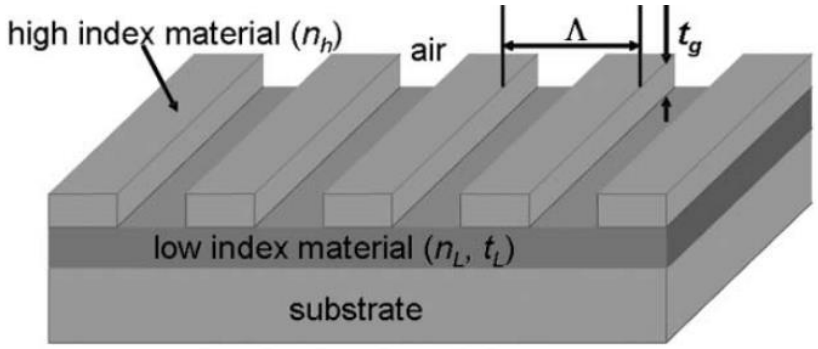

Figure 3-1: Illustration of a general SWG or High Contrast Grating highlighting the key parameters of the grating [13].

SWGs also exhibit polarization selective reflectivity which will allow our laser output to be only TE or TM light as shown in figure 2. An interesting note is that two dimensional SWGs are polarization independent due to the two dimensional symmetry through the grating structure [15]. TE and TM polarization have electric fields shifted 90 degrees from each other, which in a two dimensional grating will have the electric field and magnetic field in the same directions relative to the grating bars. While two dimensional gratings are not the focus of this thesis they could possess interesting properties to examine in future work.

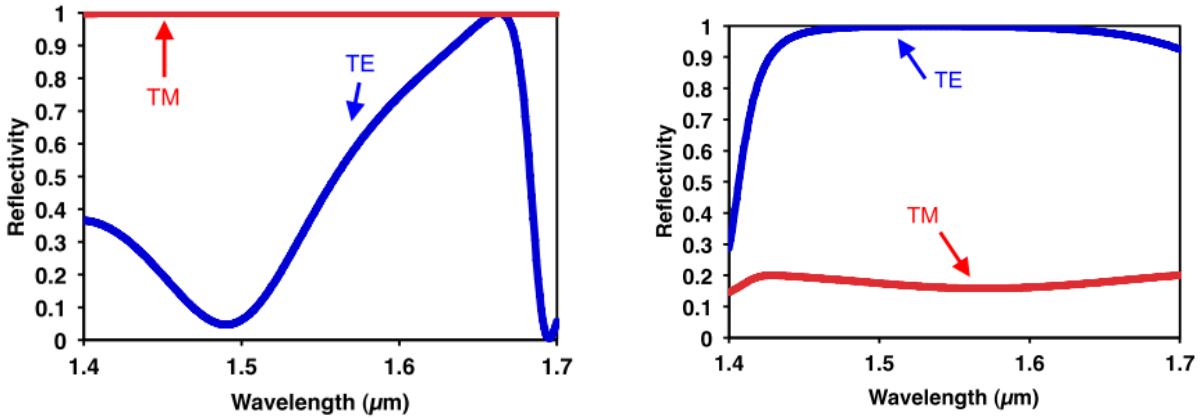

Figure 3-2: Data of two different one dimensional SWGs focused on reflecting TM light (left) and TE light (right). Highlights the polarization dependent reflectivity of each [19].

3.2. SWG for VCSELs

SWGs are a remarkable alternative reflector due to the properties discussed in this chapter. VCSELs require incredibly high reflective mirrors to have practical threshold current densities, which SWGs reliably achieve. SWGs are also much shorter than standard DBRs allowing minimal light loss through material imperfections, as well as less resistance as will be discussed later. Lastly polarization selectivity is a property DBRs do not possess, which can provide further uses that DBRs cannot. Thus, if we can apply this technology to systems where standard DBRs are inefficient, such as GaN VCSELs, a new realm of practical blue light emitting VCSELs will be opened.

4. III-Nitride VCSELs

4.1. Prospects of III-Nitride VCSELs

In the past few decades III-Nitride materials have shown themselves to be the forefront of research in UV and blue light emitting LEDs and lasers due to material advantages such as low threshold currents [23], ultra-high wear rates in low humidity conditions [24], and long active use lifetimes [25]. Blue LEDs and lasers are necessary for advances in fields such as data transfer, power efficient lighting, and displays because of their material advantages. III-Nitride lasers and LEDS are impactful enough that the advancement of III-Nitride blue LED efficiency via improvement of p-type doping and hetero junctions won Shuji Nakamura, Hiroshi Amano, and Isamu Akasaki a Nobel prize [26].

All III-Nitride semiconductors can be practically grown via Metal Organic Chemical Vapor Deposition (MOCVD) or Molecular Beam Epitaxy (MBE) systems. MOCVDs and MBEs have been the main systems for growth of all III-V semiconductors for decades. Some MOCVDs can grow on multiple wafers simultaneously allowing for mass production of semiconductor devices, allowing the III-Nitride semiconductor industry to quickly grow since its inception.

Figure 1 shows an example of a MOCVD system used to grow III-V semiconductors. III-Nitride materials have a hexagonal crystal structure, thus these semiconductors need to be grown on similar crystal structures with little lattice constant mismatch to minimize the defect density during growth. III-Nitrides are commonly grown on sapphire substrates which are loaded into the MOCVD through the loadlock chamber which can be seen on the right in figure 1 with a

large glass window. The wafer is then moved from the loadlock chamber to the growth chamber which operates at ~100-300 torr. Metal organic sources are flown in through pipes carrying, for example, Tri-methyl Gallium (TMGA) or ammonia (NH_3) as the Gallium and nitrogen sources respectively. The metal organic sources are carried to the growth chamber by inert carrier gases, either Nitrogen or Hydrogen. Growths are performed at temperatures ranging from 600^0C – 1060^0C for varying material systems and purposes.

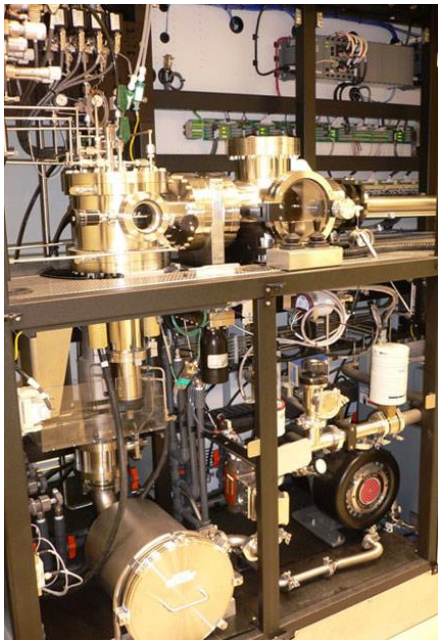

Figure 4-1: A photograph of a MOCVD system designed for single wafer growth. The growth chamber has metal organic sources sent in through piping [31]. Sources are the desired III metal attached to an ethyl or methyl group and ammonia.

4.2. Obstacles for Practical III-Nitride VCSELs

As discussed in the VCSELs section an instrumental part of the threshold current density of any laser is good mirror reflectivity. Semiconductor lasers have become heavily reliant on DBRs as mirrors for both the total reflective mirror and the exit plane mirror because they're practically

grown or fabricated and exhibit high reflectivity. These quarter-wave stack dielectric mirrors exhibit ultra-high reflectivity with a suitable number of pairs (~20-50) depending on the index contrast between the pair. GaAs VCSELs have seen much success due to practically grown DBRs utilizing GaAs and AlAs pairs. GaAs and AlAs pairs are an excellent choice for GaAs VCSEL DBRs due to a large difference of index of refractions as well as a minimal lattice constant ($\Delta a/a$ ~ .127 %) mismatch. A large difference of index of refraction allows less pairs of DBRs to be grown to achieve suitable reflectivity and a small lattice constant mismatch results in a low dislocation density throughout the DBR system for good quality crystal growth. Figure 2 shows an example of the excellent reflectivity obtained from a large number of pairs of GaAs based DBRs.

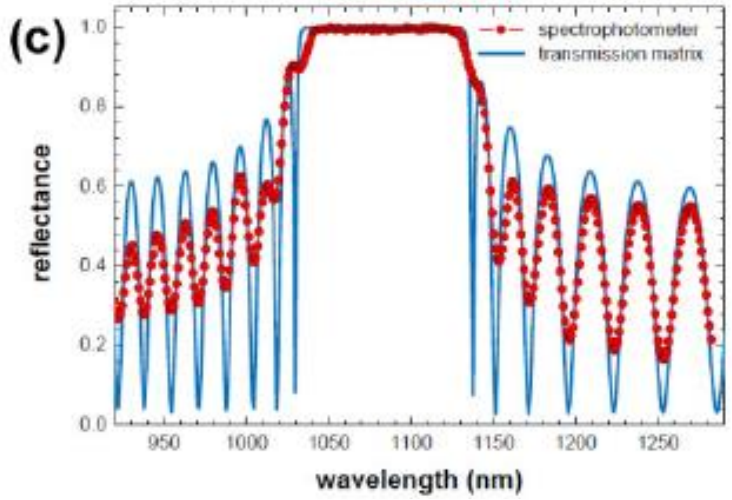

Figure 4-2: GaAs/$Al_{.92}Ga_{.08}As$ DBR reflectivity of light of wavelength near 1 μm. The mirror used contains 40 pairs with a total thickness near 7 μm [32].

III-Nitride materials however, have been struggling to find the same success in the laser industry as III-Arsenide lasers even though they possess many material advantages. This can be attributed to two key obstacles imbedded in III-Nitride materials which are lower p-type doping compared to III-Arsenide materials as well as limited reflectivity in DBRs as low as ~95 % [27]. III-Nitrides grown with unintentional doping naturally become n-type resulting in difficulties

growing material with large hole densities. GaN and AlN pairs are poor choices for DBRs due to a low index of refraction contrast and a large lattice mismatch ($\Delta a/a$ ~ 2.5 %). The large lattice mismatch results in an extremely high dislocation density, visible cracking through the structure, and strain relaxation in the system. Figure 3a shows a comparison of GaN/AlGaN DBR reflectivity for a large number of pairs between experimental results and simulation results. There is a large disparity in reflectivity between the simulation and experimental results for III-Nitride DBRs. The simulated results do not take crystal quality into consideration resulting in ultra-high reflectivity for the III-Nitride system. The measured results show the effect poor crystal quality due to defects have on DBR reflectivity. Figure 3b shows an SEM of multiple pairs of AlN/AlGaN DBRs. Highlighting the cracks propagating throughout the system.

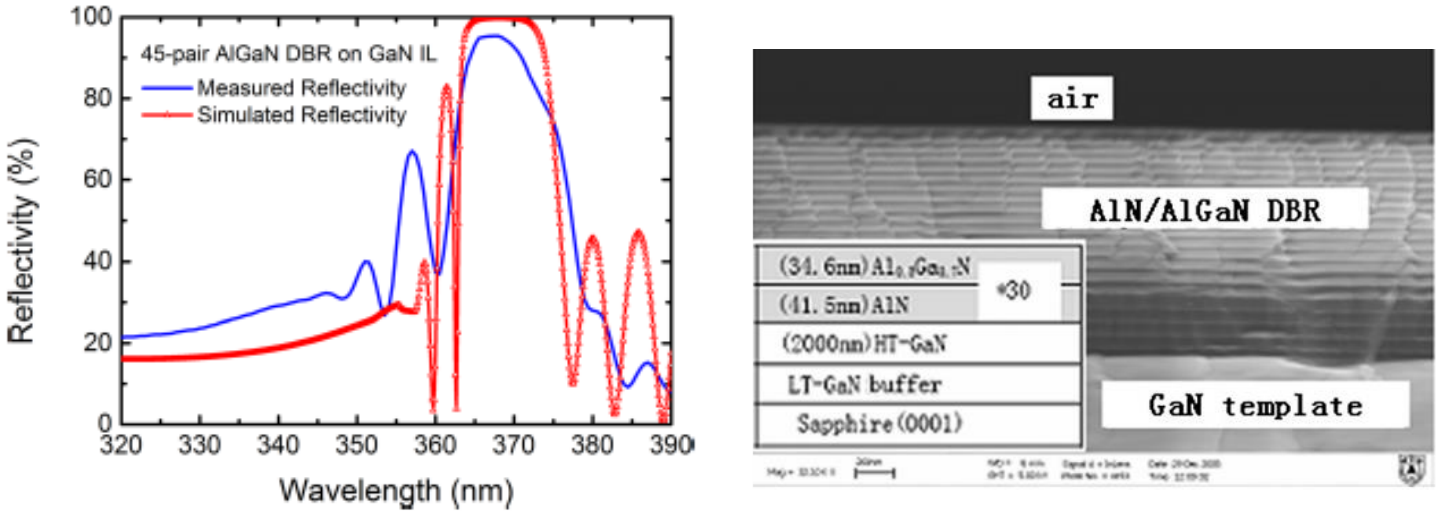

Figure 4-3: a. 45 pairs of $Al_{.30}Ga_{.70}N/Al_{.04}Ga_{.96}N$ DBRs measure and simulated reflectivity at a wavelength of λ ~370 nm. Simulated results give ultra-high reflectivity while measured is limited to ~ 95 % [27]. b. SEM showcasing the cracking due to lattice mismatch in III-Nitride DBR structure [33].

Without a suitable reflectivity for III-Nitride VCSEL mirrors the threshold current density of these systems is immensely larger than III-Arsenide systems. The low p-type doping in III-Nitride materials increases the threshold current density as well due to an increase in series

resistance. While the effect of series resistance is not present in the threshold current analysis equations shown earlier, it has a large effect in experiment. Suitable p-type doping increases the rate of holes recombining with carriers in the active region for a specific current, without enough holes the recombination rate decreases and more current will be required. While this work does not focus on solving the p-type doping obstacle, the replacement of 20-50 pairs of DBRs with a subwavelength grating mirror will result in a much lower series resistance. 20-50 pairs of DBRs can be multiple microns of material that current travels through that builds resistance. Abrupt interfaces in DBRs also builds series resistance due to an electric field created at each interface [28]. This resistance is mitigated by gradually increasing the doping from the center of the dielectric to the interfaces, however this is also difficult to achieve in III-Nitride materials as opposed to III-Arsenide materials.

4.3. Alternative Solutions to III-Nitride VCSELs

There are other possible solutions to the III-Nitride VCSEL problem. While GaN/AlN DBRs are not suitable for laser purposes due to a large lattice mismatch, possible growth of GaN/AlInN DBRs can be lattice matched with properly chosen rations of Aluminum and Indium [5][29]. This method has shown threshold current densities as low as 17 kA/cm^2. However, AlInN is difficult to grow effectively because at the temperatures that AlN is grown the Indium evaporates rapidly. Conversely at the temperatures InN is grown the AlN growth rate is too slow. While these DBRs have shown a great effect on the practicality of III-Nitride VCSELs the impact is not great enough to bring III-Nitrides to the level of the established III-Arsenide VCSELs. Alternatively, there are also III-Nitride based SWGs which solves all DBR based obstacles for GaN based VCSELs.

5. III-Nitride SWGs

5.4. Our III-Nitride SWG

The III-Nitride SWG this work focuses on is shown in figure 1. The SWG is a GaN grating surrounded by air that is implemented into our VCSEL via a membrane structure. The target reflected wavelength is 450 nm with TE polarizations (E parallel to grating bars) which is practically achievable by InGaN quantum well systems. This design is only viable for the top mirror of a VCSEL because no stable structure needs to be in place for further growth above the grating. SWGs implemented as a bottom mirror are not the focus of this work and will require more creativity to implement because after growth and fabrication of the bottom SWG there will be a need to continue the VCSEL growth on the grating. There are various material combinations that can be achieved in this membrane structure such as varying the air gap with an oxide layer, replacing GaN with AlN, etc. A GaN grating surrounded by air was chosen because this design can be conveniently grown by a MOCVD system where the rest of the VCSEL structure will also be grown and GaN is transparent to blue light.

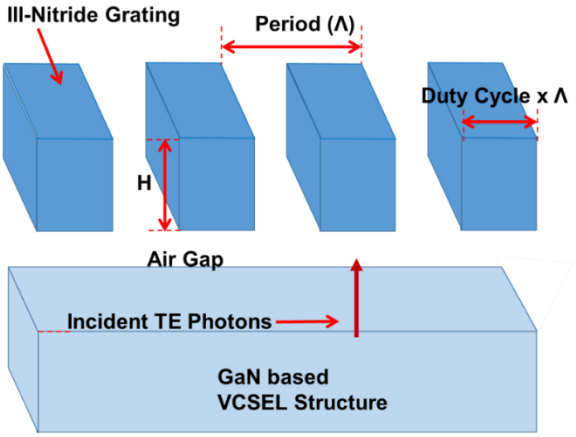

Figure 5-1: Illustration of our proposed implemented III-Nitride SWG highlighting the duty cycle, period, air gap and height. This grating is designed to reflect only TE photons which have an electric field parallel to the grating bars.

There exist other variations on SWGs such as the Zero Contrast Grating [20] which pushes the index contrast further than the grating/substrate interface, allowing the light to travel further past the grating before being reflected and also results in ultra-high reflectivity. We currently feel that this method presents too much variance without a suitable amount of increase in reflectivity to be used in our blue light reflecting SWG design.

It has been shown that the parameters of an SWG and its reflectivity are perfectly scalable assuming constant index of refractions [15]. This effect can prove to be useful when designing a new grating in a nearby spectral regime, however in practice it can be impractical to utilize for far spectral regimes due to large differences of index of refractions with varying wavelengths. This effect is shown in this thesis in figure 2, where we double the physical dimensions of our GaN SWG as well as double the wavelength regime. The shapes of the reflective bands are near identical, though the center band reflection for the doubled regime is slightly lower than the original grating in the center with R ~ 99.3 % as opposed to 99.99 %.

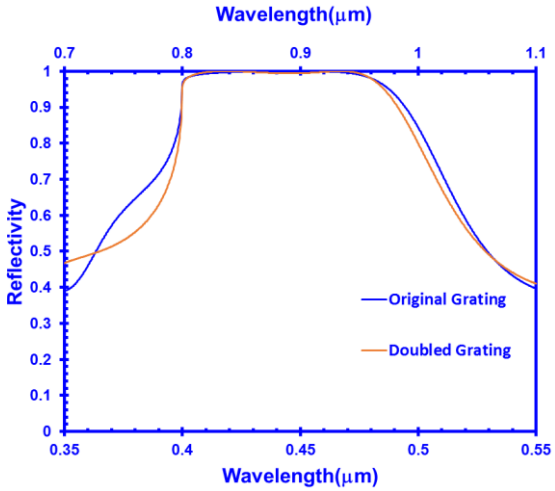

Figure 5-2: The reflectivity of the original stated GaN grating (blue) and the reflectivity of the GaN grating with doubled physical dimensions (orange).

The GaN based SWG examined in this work possesses a grating height of 130 nm, a period of 400 nm, a duty cycle of 50 %, and an airgap of 200 nm. This design exhibits ultra-high reflectivity (R > 99 %) with a $\Delta\lambda/\lambda$ ~ 17.8% for TE light. As shown in figure 2 the same grating reflecting TM light exhibits a much narrower reflection bandwidth than the TE band so this SWG is also polarization dependent. The extremely low TM light reflectivity for a laser will not allow TM light to lase in a SWG implemented VCSEL until threshold currents are far beyond what is necessary.

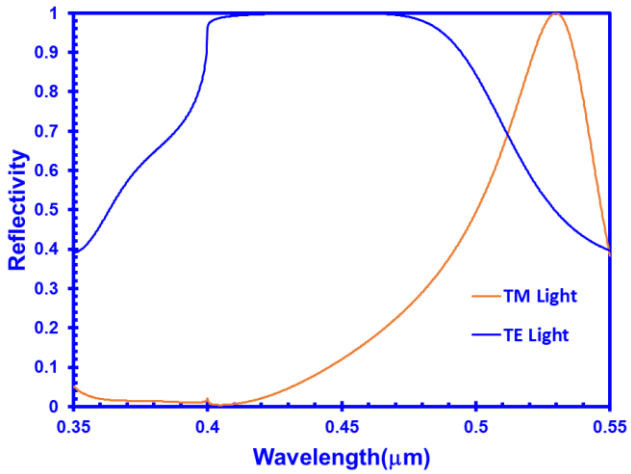

Figure 5-3: The reflectivity of TE and TM light for a GaN based SWG with H = 130 nm, Λ = 400 nm, and duty cycle of 50 %. The grating is designed to reflect TE light and is thus polarization selective.

5.2. Effects of Grating Parameters on Grating Reflectivity

The period of a reflecting SWG must be smaller than the desired reflected wavelength, if this condition is not met the grating reflectivity decreases dramatically. Figures 2a and 2b show the reflectivity of our GaN membrane grating surrounded by air as functions of wavelength and

period. Figure 2a shows the reflective band for multiple SWGs with varying periods from 360 nm to 440 nm. From figure 2a we can see the position of reflective band relies heavily on the period of the grating where a period of 400 nm maintains R>99% for a minimum wavelength of 400 nm. As the period increases or decreases the band position will also increase or decrease. Figure 2b highlights that for this grating there is a linear relationship between the minimum wavelength capable of high reflectivity and the period of the grating. We can utilize this relationship in the future to aid designing SWGs in various spectral regimes. The shape and reflectivity of this SWG are very resilient to a change in grating period, which will make this SWG more practical to consistently fabricate with the high reflective property we desire. Given a constant height and duty cycle the reflectivity at a wavelength of 450 nm is larger than 99% for all periods in the range of ~390 nm to ~450 nm. The period has a tolerance of $\Delta\Lambda/\Lambda$~ 14.3% which allows us to achieve ultra-high reflectivity with a very large range for error in fabrication. It will be shown that the period of the grating has the largest fabrication tolerance of any grating parameter.

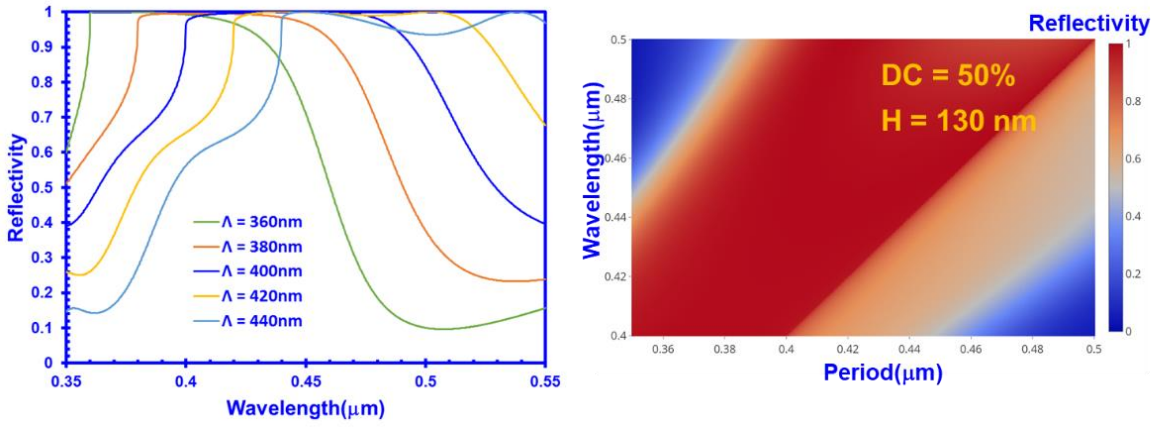

Figure 5-4: a) Grating reflectivity for varying periods from 360 nm – 440 nm. The height is held constant at 130 nm and duty cycle at 50%. b) Surface plot of grating reflectivity for continuously varying periods from 350 nm – 500 nm.

There is an inverse relationship between the reflective bandwidth and the value of the grating height and duty cycle. We found that the height and the duty cycle of the grating have a significantly lower fabrication tolerance than the grating period. From figure 3a we see that a 4% change in the duty cycle can decrease the reflectivity by more than 10%. The recorded range of ultra-high reflectivity (R > 99%) for the duty cycle of the grating is from ~0.48 to ~0.51, which is a tolerance of a 6% change in duty cycle. There is a tolerance of 12 % for the height which has a high reflective bandwidth from 123 nm to 139 nm which is twice as tolerant as the duty cycle. While in practice the variations in period, duty cycle, and height won't be constant throughout the grating this data still provides insight on the resilience of each grating parameter. Experimental work has been done on infrared SWGs confirming similar period and grating spacing resilience [11]. However, the duty cycle and height do not exhibit a clear trend that can be utilized for prediction of values necessary for high reflection in a given spectral regime.

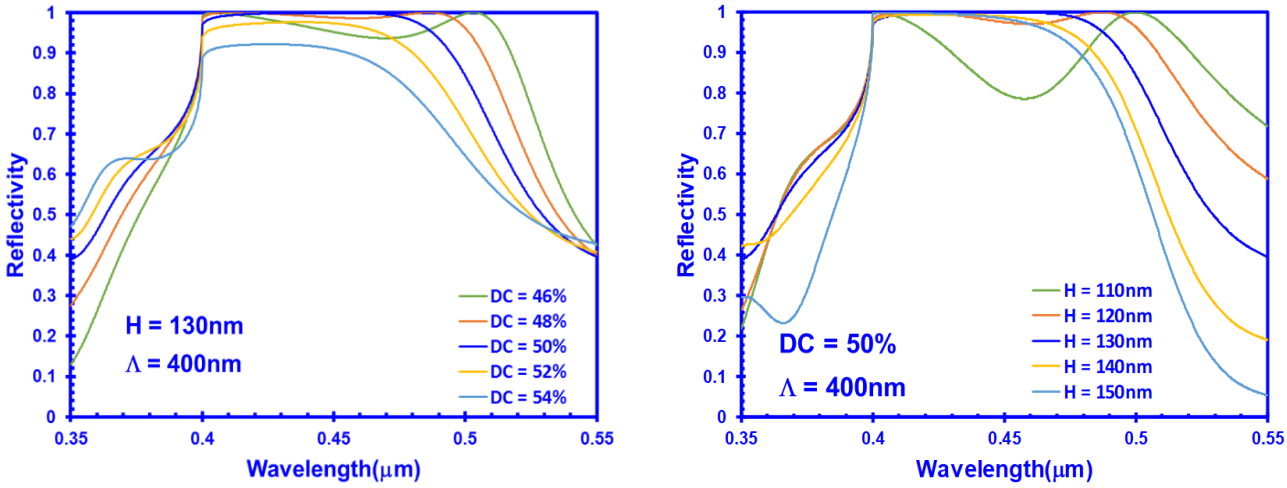

Figure 5-5: a) Grating reflectivity for varying duty cycles from 46% – 54%. The height is held constant at 130 nm period at 400 nm. b) Grating reflectivity for varying heights from 110 nm – 150 nm. The period is held constant at 400 nm and the duty cycle at 50%.

5.3. Threshold Analysis of Implemented SWG III-Nitride VCSEL

To understand the numerical effect implementing an SWG has on the performance of a VCSEL we need to perform a threshold analysis. The lower the threshold current density is the more practical these VCSELs will lase with standard power supplies. This analysis was performed by replacing the top mirror of a standard DBR implementing in a III-Nitride VCSEL with a highly reflective SWG. In this threshold current density analysis, we varied the bottom mirror reflectivity between 99.99 % and 99.95 % while using the same top mirror SWG for each calculation. GaN/AlN DBRs are not capable of achieving these levels of bottom mirror reflectivity and an alternative reflector will be required to obtain these results.

Table 1: Threshold analysis intrinsic parameter assumptions for a standard InGaN QW VCSEL are shown [34]–[37]. These parameters include the loss parameters of the system, structural parameters, and the gain parameters.

Threshold Analysis Parameters for InGaN QW VCSEL Structure							
A	**B**	**C**	**n_{tr}**	**Γ**	**g_{0n}**	**α_i**	**T**
$10^9\ s^{-1}$	$5X10^{-11}\ cm^3s^{-1}$	$10^{-30}\ cm^6s^{-1}$	$1.8X10^{19}\ cm^{-3}$	0.0216	1360 cm^{-1}	8.6 cm^{-1}	4 nm

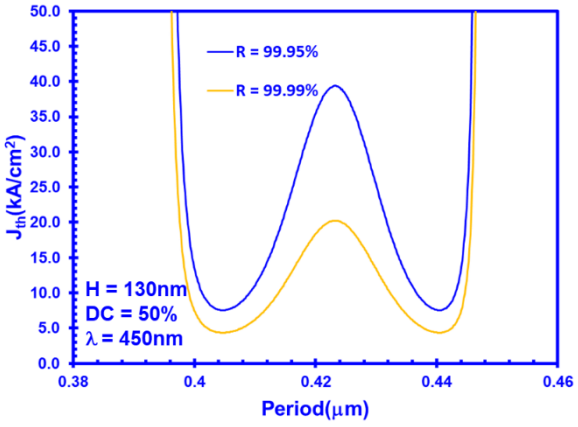

Figure 5-6: Threshold current density based on grating period of implemented SWG VCSEL structure for variable bottom mirror reflectivity ranging from 99.95% to 99.99%.

From equations 1.2-4, 1.2-5, and 1.2-6 we can gain an understanding of our VCSEL's threshold current density where Γ = T/L. Keeping our GaN/Air SWG reflector with a duty cycle of 50% and height of 130 nm for an active region emitting light at a wavelength of 450 nm we can see the threshold current density in figure 4 as it depends on grating period. A practical bottom mirror is just as necessary as a practical top mirror, without both practical threshold current densities may never be reached. However, with an exceptional bottom mirror implemented as well as our SWG reflector threshold current densities as low as ~4.6 kA/cm^2 are achievable. The recent advances in experimental III-Nitride VCSELs utilizing AlInN DBRs have shown threshold currents as low at 17 kA/cm^2 [29], which clearly shows properly implemented SWGs can compete with other III-Nitride VCSEL advances even if we arbitrarily lowered the grating reflectivity to account for experimental error. The effect of the grating period's large fabrication tolerance can be seen by how wide the bandwidth of the threshold current density is, however the effect of a slightly less reflective center is apparent with the larger threshold current density. As expected, once the period exceeds that tolerance the threshold current density will increase dramatically. We can expect plotting the threshold current density as it depends on height and duty cycle will look narrower. The center of the band is at a period of 420 nm with a threshold current density of ~ 20 kA/cm^2 which is considerably larger. Utilizing the same threshold analysis with conventional GaN/AlN DBRs as the top and bottom mirrors with maximum reflectivity of 95% gives threshold current densities as high as 3X10^9 kA/cm^2. The exceptionally low threshold current densities via SWG reflector implementation can result in practical blue emitting III-Nitride VCSELs as long as a practical alternative reflector for the bottom mirror can be achieved as well.

5.4. Future Work for III-Nitride SWGs

As this is all theoretical work, the first thing that should be done is fabrication of our GaN/Air SWG. Figure 5 shows an illustration of the fabrication process of a membrane structure SWG reflector once the p-type DBRs have been grown. Post growth of 3-5 pairs of p-type DBRs an oxide pattern for selective area epitaxy (SAE) must be deposited on the structure with the desired airgap height. Following the oxide deposition, GaN growth can begin and continue until the lateral epitaxy overgrowth of the GaN has sufficiently surrounded the oxide deposition with a height larger than the desired grating height. The structure can be brought to a clean room for patterning and ICP etching to create the grating formation once the GaN growth has completed, then the membrane structure is formed by removing the oxide layer via wet etching processes. Other future work should be done on the effects of leaving the oxide layer under the grating as opposed to the air gap, as well as fiddling with various material gratings for reflection in the blue light spectral regime.

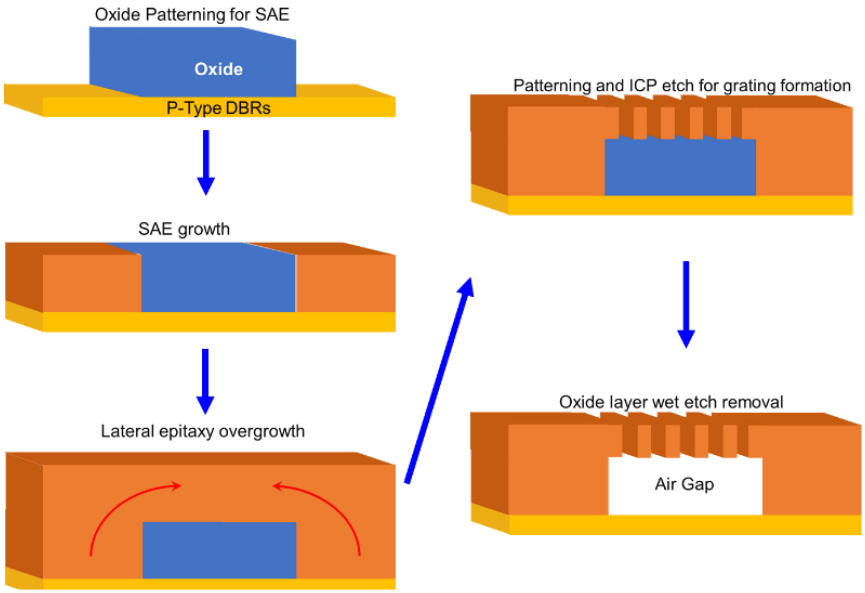

Figure 5-7: An Illustration of a proposed fabrication and implementation processes of a GaN based SWG post growth of 3-5 pairs of p-type DBRs.

For example, using AlN with an SiO_2 layer left underneath in the same membrane formation can lead to similarly high reflectivity. This AlN/oxide grating has a height of 225 nm, a period of 370 nm, an SiO_2 height of 90 nm, and a duty cycle of 80 %. The reflectivity is shown in figure 6 for this grating. The reflective band does consistently maintain reflections above 99 % however the $\Delta\lambda/\lambda$ ~ 21.7% for R > 98 %. Thus, the oxide gratings may prove to be as effective as the air gap SWGs which will be necessary for the bottom mirror where an airgap may not be possible.

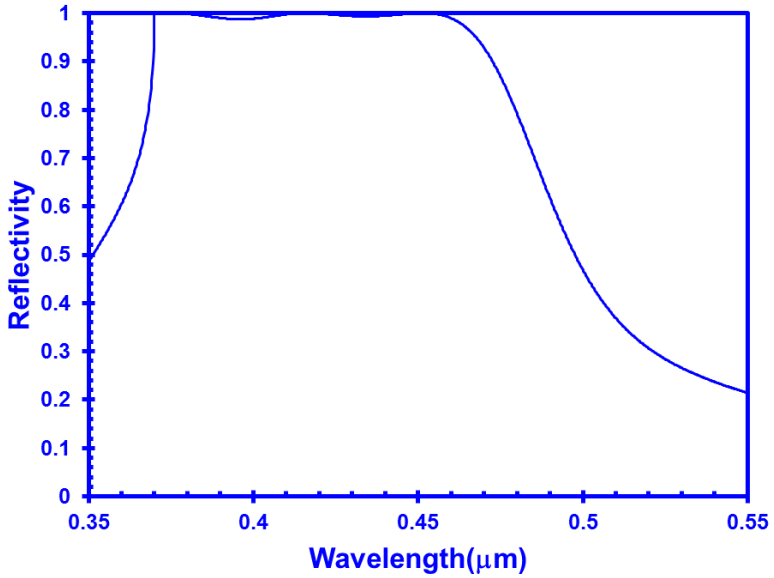

Figure 5-8: The reflective of an AlN/SiO_2 grating with H = 225 nm, Λ = 370 nm, duty cycle = 80 %, and SiO_2 height of 90 nm.

Due to the small physical dimensions of SWGs mass production may be a problem in the future without a suitable robustness in the grating design. GaAs SWGs reflect light in the infrared spectrum which is about 1 um, while blue reflecting SWGs will be on the order of a few hundreds of nanometers. Given this, finding an SWG with an exceptional fabrication tolerance is one of the hurdles that needs to be crossed.

6. **Conclusion**

In conclusion, SWGs were shown to be an exceptional alternative to standard GaN/AlN DBRs in blue emitting VCSELs. GaN SWGs can exhibit ultra-high reflection in the blue light spectral regime that III-Nitride DBRs cannot. The fabrication tolerance as well as the effect of change of grating parameters were studied and demonstrated. The period of the grating was shown to have the greatest fabrication tolerance of the grating parameters as well as play a key role in determining the position of the reflective band. We have performed a threshold analysis on multiple VCSELs implementing our GaN SWG with variable bottom mirror reflectivity. Utilizing a GaN SWG with a suitable bottom mirror was shown to achieve threshold current densities as low as 4.6 kA/cm^2.

Practical blue and UV VCSELs have been shown to be achievable by implementation of SWG technology. We have shown that an AlN/SiO_2 SWG can also achieve ultra-high reflectivity in the blue light emitting spectral regime, which can be useful for UV light emission where GaN is no longer transparent. Designing possible alternative bottom mirror SWGs is a potential future endeavor as well. Bottom mirror SWGs may be implemented via oxide deposition and SAE growth where the deposited oxide will be the grating bars. This work is one of many possible SWG implementations that can be utilized for blue emitting III-Nitride VCSELs, and there may be many more exceptional SWG reflectors to be found. Thus, it is likely SWGs can lead a path towards practical and efficient blue emitting III-Nitride VCSELs.

References

[1] K. Iga, “Vertical-cavity surface-emitting laser: Its conception and evolution,” *Jpn. J. Appl. Phys.*, vol. 47, no. 1, pp. 1–10, 2008.

[2] H. Soda, K. Iga, C. Kitahara, and Y. Suematsu, “GaInAsP / InP Surface Emitting Injection Lasers,” *Jpn. J. Appl. Phys.*, vol. 18, no. 12, pp. 2329–2330, 1979.

[3] I. of M. and Optoelectronics, P. D. Of, and T. S. F. S. lasers book Institute, *Semiconductor Lasers I Fundamentals*, no. 1. 2014.

[4] R. S. Geels and L. A. Coldren, “Laser Diodes,” *October*, vol. 1605, no. May 2011, pp. 1–3, 1990.

[5] R. Butté *et al.*, “Current status of AlInN layers lattice-matched to GaN for photonics and electronics,” *J. Phys. D. Appl. Phys.*, vol. 40, no. 20, pp. 6328–6344, 2007.

[6] R. J. D. Tilley, *Colour and the Optical Properties of Materials*. 2011.

[7] P. Mackowiak and W. Nakwaski, “Detailed threshold analysis of UV-emitting nitride vertical-cavity surface-emitting lasers,” *J. Phys. D. Appl. Phys.*, vol. 31, pp. 2479–2484, 1998.

[8] M. G. Moharam, E. B. Grann, D. a. Pommet, and T. K. Gaylord, “Formulation for stable and efficient implementation of the rigorous coupled-wave analysis of binary gratings,” *J. Opt. Soc. Am. A*, vol. 12, no. 5, p. 1068, 1995.

[9] M. G. Moharam, D. A. Pommet, E. B. Grann, and T. K. Gaylord, “Stable implementation of

the rigorous coupled-wave analysis for surface-relief gratings: enhanced transmittance matrix approach," *J. Opt. Soc. Am. A*, vol. 12, no. 5, p. 1077, 1995.

[10] L. Li, "Use of Fourier Series in the analysis of discontinuous periodic structures," *J. Opt. Soc. Am A*, vol. 13, no. 9, pp. 1870–1876, 1996.

[11] Y. Zhou, M. C. Y. Huang, and C. J. Chang-Hasnain, "Large fabrication tolerance for VCSELs using high-contrast grating," *IEEE Photonics Technol. Lett.*, vol. 20, no. 6, pp. 434–436, 2008.

[12] C. J. Chang-Hasnain, "Tunable VCSEL," *IEEE J. Sel. Top. Quantum Electron.*, vol. 6, no. 6, pp. 978–987, 2000.

[13] C. F. R. Mateus, M. C. Y. Huang, L. Chen, C. J. Chang-Hasnain, and Y. Suzuki, "Broad-band mirror (1.12-1.62 μm) using a subwavelength grating," *IEEE Photonics Technol. Lett.*, vol. 16, no. 7, pp. 1676–1678, 2004.

[14] C. Chang-Hasnain and W. Yang, "High-contrast gratings for integrated optoelectronics," *Adv. Opt. Photon.*, vol. 4, no. 3, pp. 379–440, 2012.

[15] C. F. R. Mateus, M. C. Y. Huang, Y. Deng, A. R. Neureuther, and C. J. Chang-Hasnain, "Ultrabroadband Mirror Using Low-Index Cladded Subwavelength Grating," *IEEE Photonics Technol. Lett.*, vol. 16, no. 2, pp. 518–520, 2004.

[16] T. Ansbaek, I. S. Chung, E. S. Semenova, and K. Yvind, "1060-nm tunable monolithic high index contrast subwavelength grating VCSEL," *IEEE Photonics Technol. Lett.*, vol. 25, no. 4, pp. 365–367, 2013.

[17] Y. Zhou *et al.*, “High-index-contrast grating (HCG) and Its applications in optoelectronic devices,” *IEEE J. Sel. Top. Quantum Electron.*, vol. 15, no. 5, pp. 1485–1499, 2009.

[18] V. Karagodsky, F. G. Sedgwick, and C. J. Chang-Hasnain, “Theoretical analysis of subwavelength high contrast grating reflectors,” *Opt. Express*, vol. 18, no. 16, p. 16973, 2010.

[19] C. Chase, “High Contrast Grating VCSELs : Properties and Implementation on InP-based VCSELs,” *PhD thesis*, 2011.

[20] R. Magnusson, “Wideband reflectors with zero-contrast gratings.,” *Opt. Lett.*, vol. 39, no. 15, pp. 4337–40, 2014.

[21] I. S. Chung, J. Mørk, P. Gilet, and A. Chelnokov, “Subwavelength grating-mirror VCSEL with a thin oxide gap,” *IEEE Photonics Technol. Lett.*, vol. 20, no. 2, pp. 105–107, 2008.

[22] T. T. Wu *et al.*, “Sub-wavelength GaN-based membrane high contrast grating reflectors.,” *Opt. Express*, vol. 20, no. 18, pp. 20551–7, 2012.

[23] S. Nakamura *et al.*, “Continuous-wave operation of InGaN/GaN/AlGaN-based laser diodes grown on GaN substrates,” *Appl. Phys. Lett.*, vol. 72, no. 16, pp. 2014–2016, 1998.

[24] G. Zeng, C. K. Tan, N. Tansu, and B. A. Krick, “Ultralow wear of gallium nitride,” *Appl. Phys. Lett.*, vol. 109, no. 5, pp. 1–6, 2016.

[25] S. Nakamura *et al.*, “High-Power , Long-Lifetime InGaN / GaN / AlGaN-Based Laser Diodes Grown on Pure GaN Substrates,” *Jpn. J. Appl. Phys.*, vol. 37, no. 3, pp. L309–L312, 1998.

[26] “The 2014 Nobel Prize in Physics - Press Release.” [Online]. Available:

https://www.nobelprize.org/nobel_prizes/physics/laureates/2014/press.html. [Accessed: 01-Nov-2017].

[27] Y. Liu *et al.*, "Strain management of AlGaN-based distributed Bragg reflectors with GaN interlayer grown by metalorganic chemical vapor deposition Strain management of AlGaN-based distributed Bragg reflectors with GaN interlayer grown by metalorganic chemical vapor deposi," vol. 81103, no. 2016, 2016.

[28] K. Tai, L. Yang, Y. H. Wang, J. D. Wynn, and A. Y. Cho, "~ EC L-J LEe," vol. 2496, no. 1990, pp. 1–4, 2001.

[29] K. Matsui *et al.*, "GaN-based vertical cavity surface emitting lasers with periodic gain structures," *Jpn. J. Appl. Phys.*, vol. 55, no. 5, 2016.

[30] L. A. Coldren and S. W. Corzine, *Diode Lasers and Photonic Integrated Circuits*. 2012.

[31] "Lehigh CPN: MOCVD Epitaxy & Synthesis Lab." [Online]. Available: http://www.lehigh.edu/~incpn/research/facilities/mocvd.html. [Accessed: 02-Nov-2017].

[32] G. D. Cole, W. Zhang, M. J. Martin, J. Ye, and M. Aspelmeyer, "Tenfold reduction of Brownian noise in high-reflectivity optical coatings," *Nat. Photonics*, vol. 7, no. 8, pp. 644–650, 2013.

[33] Z. L. Xie *et al.*, "High reflectivity AlGaN/AlN DBR mirrors grown by MOCVD," *J. Cryst. Growth*, vol. 298, no. 1, pp. 691–694, 2007.

[34] J. Piprek, "Efficiency droop in nitride-based light-emitting diodes," *Phys. Status Solidi Appl. Mater. Sci.*, vol. 207, no. 10, pp. 2217–2225, 2010.

[35] H. Zhao and N. Tansu, “Optical gain characteristics of staggered InGaN quantum wells lasers,” *J. Appl. Phys.*, vol. 107, no. 11, 2010.

[36] C. Tan, W. Sun, D. Borovac, and N. Tansu, “Large Optical Gain AlInN-Delta- GaN Quantum Well for Deep Ultraviolet Emitters,” *Nat. Publ. Gr.*, no. February, pp. 1–7, 2016.

[37] E. Kioupakis, P. Rinke, K. T. Delaney, and C. G. Van De Walle, “Indirect Auger recombination as a cause of efficiency droop in nitride light-emitting diodes,” *Appl. Phys. Lett.*, vol. 98, no. 16, 2011.

Vita

Austin M. Slosberg was born on February 21, 1994 in Belle Harbor, NY to Mark and Lisa Slosberg. He entered the University of Rochester in 2012 and graduated with a Bachelor's of Science in Physics with a minor in Mathematics. Afterwards, he started his graduate studies in Electrical Engineering at Lehigh University under his adviser Professor Nelson Tansu in 2016. With this thesis, he will graduate with a Master's of Science in Electrical Engineering in December 2017.